Peptoids as Chiral Stationary Phase for Liquid Chromatography: Insights from Molecular Dynamics Simulations

Sébastien Hoyas,[a,b] Otello M. Roscioni,[c,d] Corentin Tonneaux,[a] Pascal Gerbaux,[b] Jérôme Cornil,[a] Luca Muccioli[c]**

[a] Laboratory for Chemistry of Novel Materials, Center of Innovation and Research in Materials and Polymers, Research Institute for Science and Engineering of Materials, University of Mons, 23 Place du Parc, 7000 Mons, Belgium

[b] Organic Synthesis & Mass Spectrometry Laboratory, Interdisciplinary Center for Mass Spectrometry (CISMa), Center of Innovation and Research in Materials and Polymers (CIRMAP), University of Mons, 23 Place du Parc, 7000 Mons, Belgium

[c] Department of Industrial Chemistry « Toso Montanari », University of Bologna, Viale Risorgimento 4, 40136 Bologna, Italy

[d] MaterialX LTD, Bristol BS2 0XJ, UK

chiral stationary phase, enantioselectivity, helix, molecular dynamics, peptoid

Abstract

Peptoids are peptide regioisomers with attractive structural tunability in terms of sequence and three-dimensional arrangement. Peptoids are foreseen a great potential for many diverse applications, including their utilization as chiral stationary phase in chromatography. To achieve chiral recognition, a chiral side chain is required to allow specific interactions with a given enantiomer from a racemic mixture. One of the most studied chiral stationary phase, built with (*S*)-N-1-phenylethyl (*N*spe) units, was showed successful in resolving racemic mixtures of binaphthyl derivatives. However, there is currently no description at the atomic scale of the factors favoring its enantioselectivity. Here, we take advantage of steered molecular dynamics simulations to mimic the elution process at the atomic scale and present evidence that the predominantly right-handed helical conformation of *N*spe peptoids, and their ability to form stronger hydrogen bonds with the (*S*) enantiomer, are responsible for the chiral recognition of the popular chiral probe 2,2'-bihydroxy-1,1'-binaphthyl.

1. Introduction

The majority of biological molecules such as amino acids and proteins, carbohydrates, or hormones is chiral although only one of the two enantiomers is commonly found in living organisms.[1] In contrast, many chiral synthetic compounds such as drugs are obtained in racemic mixtures.[2] Enantiomers often display different reactivity in biological systems which are enantioselective.[3] This is particularly critical in the pharmaceutical field so that a careful control of the enantiomeric composition is mandatory to avoid medical disasters, such as the infamous thalidomide drug scandal in the late 1950s.[3] Various methods have been developed to obtain enantiopure drugs, such as Dutch resolution or asymmetric synthesis.[4,5] Using the later method,

two kinds of chiral reagents are required if both pure enantiomers are needed. Moreover, this method is limited by the high cost of the catalysts and often requires lengthy synthetic routes.[6,7] An alternative relies on the preparation and direct separation of a racemate by chiral stationary phases (CSPs) in chromatography columns.[8] Nowadays, a large diversity of CSPs is available to carry out enantioselective resolution. These CSPs mainly involve compounds such as cyclodextrins,[9] polysaccharides,[10] proteins or peptide oligomers.[11–13] In the latter case, previous studies suggested that specific secondary structures, such as a helical conformation, can promote and enhance enantioselectivity.[12–15] In 2011, Wu *et al.* investigated peptoids as a new class of chiral selector compounds in stationary phases.[16] Peptoids are peptidomimetic molecules in which the side chain is appended to the nitrogen atom of the amide group instead of the carbon in α-position to the amide carbonyl as it is the case in peptides.[17] These molecules are used in many different applications, ranging from biomedical to nanotechnology,[18,19] as well as in materials science,[20,21] because of their ease of synthesis and their resistance to proteolysis compared to their peptide analogues.[22,23] They also offer a huge versatility of structures by variation of the nature of the side chains; in particular, changing the nature of the side chain around the C terminus extremity was identified as a strategy to improve the chiral recognition.[24,25] Besides their helical conformation, peptoids have additional attractive features to achieve chiral recognition, thanks to their amide groups that can act as hydrogen bond acceptors and to the wide variety of side chains that can be introduced, such as aromatic rings to create π-π interactions with chiral molecules containing aromatic moieties. In their study, Wu *et al.* have shown that peptoids grafted via their N terminus extremity on silica do exhibit enantioselective properties against chiral binaphthyl derivatives in presence of aromatic, bulky and chiral side chain, such as the (*S*)-1-phenylethyl group (*N*spe, **Scheme 1**).[16] This enantioselectivity has been linked to the fact that peptoids bearing

*N*spe side chains start adopting a helical conformation at a length of about 5 residues, which allows the establishment of specific interactions with a given enantiomer.[16,26] There is, however, no clear description at the atomistic scale of the origin of these enantioselective properties.

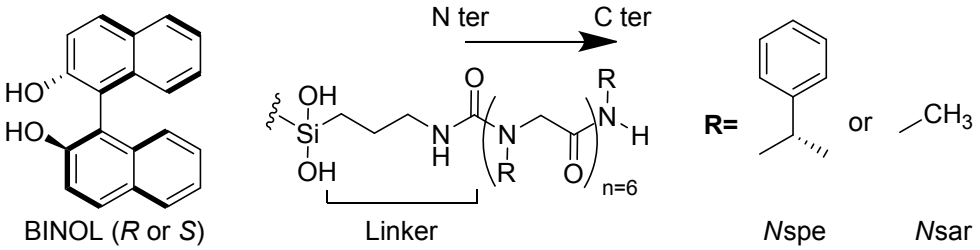

Scheme 1. Primary structure of (**A**) BINOL (*R* or *S* 2,2'-bihydroxy-1,1'-binaphthyl) and (**B**) a peptoid chain, represented from N to C terminus, with *N*spe or *N*sar side chains and its linker for grafting on silica.

This has motivated the present study which describes the process of chiral recognition of peptoids substituted by *N*spe side chains grafted on silica by means of molecular dynamics (MD) simulations. Simulations of chiral interfaces can assist experimentalists by shedding light on the recognition mechanism and the interactions involved between the selectors and the analytes to guide synthetic efforts, as recently shown for the well-known Whelk-O1 chiral stationary phase,[27,28] or even for peptides and saccharides oligomers.[29–31] To best mimic the conditions reported in the experimental study, we reproduced in our simulations key relevant parameters such as the grafting density and the solvent composition.[16] We considered a peptoid of six units bearing seven *N*spe side chains (*N*spe$_7$ referred to as CSP5 in **Ref. 16**) as host and a binaphthyl derivative as guest (2,2'-bihydroxy-1,1'-binaphthyl or BINOL), see **Scheme 1**.[16] We selected *N*spe$_7$ as the enantioselective peptoid because it displays one of the best separation factors towards (*R*)- and (*S*)-BINOL in the experiments carried out by Wu *et al*.[16] Steered molecular dynamics (SMD) have

been performed to drag the enantiomers all along the model elution column and assess on a relative basis their average velocities. Moreover, to test the validity of the computational model, we performed the same simulations using an achiral peptoid bearing methyl side chains (*N*sar) which behaves as random coil in solution (**Scheme 1**)[32] and for which the two BINOL enantiomers are expected to display identical velocities. Our simulations qualitatively reproduce the experimental trend, i.e., the (*S*)-BINOL enantiomer is retained for a longer time by the grafted *N*spe$_7$ peptoids and support the initial hypothesis that the helical structure plays a pivotal role in the enantioseparation.

2. Materials and Methods

Sample preparation

An amorphous silica bulk is first generated by heating and cooling down a crystalline supercell of cristobalite, as described elsewhere.[33,34] We then extract from this structure one slab whose surface dimensions equal to 58.7 × 58.7 Å^2, and with a thickness of about 60 Å. The slab was placed horizontally (in the xy plane) in the simulation box, with the two surfaces of the slab forming the walls of the model chromatography column, or more precisely of a single pore of the silica beads which are used in the column. Random defects were further created independently in each slab by removing SiO_2 units from the surface layers in order to increase the roughness of the otherwise atomically flat surfaces. The atomic coordinates were then relaxed to allow local surface reconstruction by thermal annealing. First, a linear ramp in temperature was applied from 300 K to 900 K for 0.5 ns (heating rate: 1.2 K/ps), followed by an annealing at 900 K for 0.5 ns, and finally cooled down to 300 K (1.2 K/ps for 0.5 ns) before a final energy minimization.[34,35] The pore size of the silica beads used by Wu *et al.* is about 100 Å,[16] whereas the gap used between the two surfaces in our simulation is instead 65 Å in order to save computational time. This is a

reasonable approximation since this thickness is large enough to ensure that peptoids grafted on opposite surfaces do not interact. The bulk structure and the surface silanol groups of silica were described using the Clay force field parameters.[36]

The surface was then decorated with a self-assembled monolayer of oligopeptoid chains. Namely, we have described the chiral *N*spe and achiral *N*sar peptoids made of 6 monomer units (**Scheme 1**) by using a previously developed parameterization of the DREIDING force field specific to peptoids (i.e., the PEPDROID force field), in which the torsional barriers were reduced artificially to allow for a proper conformational sampling at 298 K (see details in **Supporting Information**).[37] Peptoid atomic charges were set using the Gasteiger method in Materials Studio 18.0,[38,39] as described in the original paper.[37] The grafting density is about 0.36 peptoid chain/nm², similar to that reported in the experimental study of *N*spe peptoids (details in **Supporting Information**).[16] To achieve this grafting density, 10 peptoid chains (20 in total) were attached on each silica surface on randomly chosen anchoring sites by connecting them via an alkyl linker to the silanol groups, see **Figure 1**. The *N*spe peptoid hexamers are grafted on the surface (through their N terminus extremity, attached to the linker) in their right-handed helical conformation, using the same initial conformation as described in the theoretical study performed by Armand *et al.*[16,40]

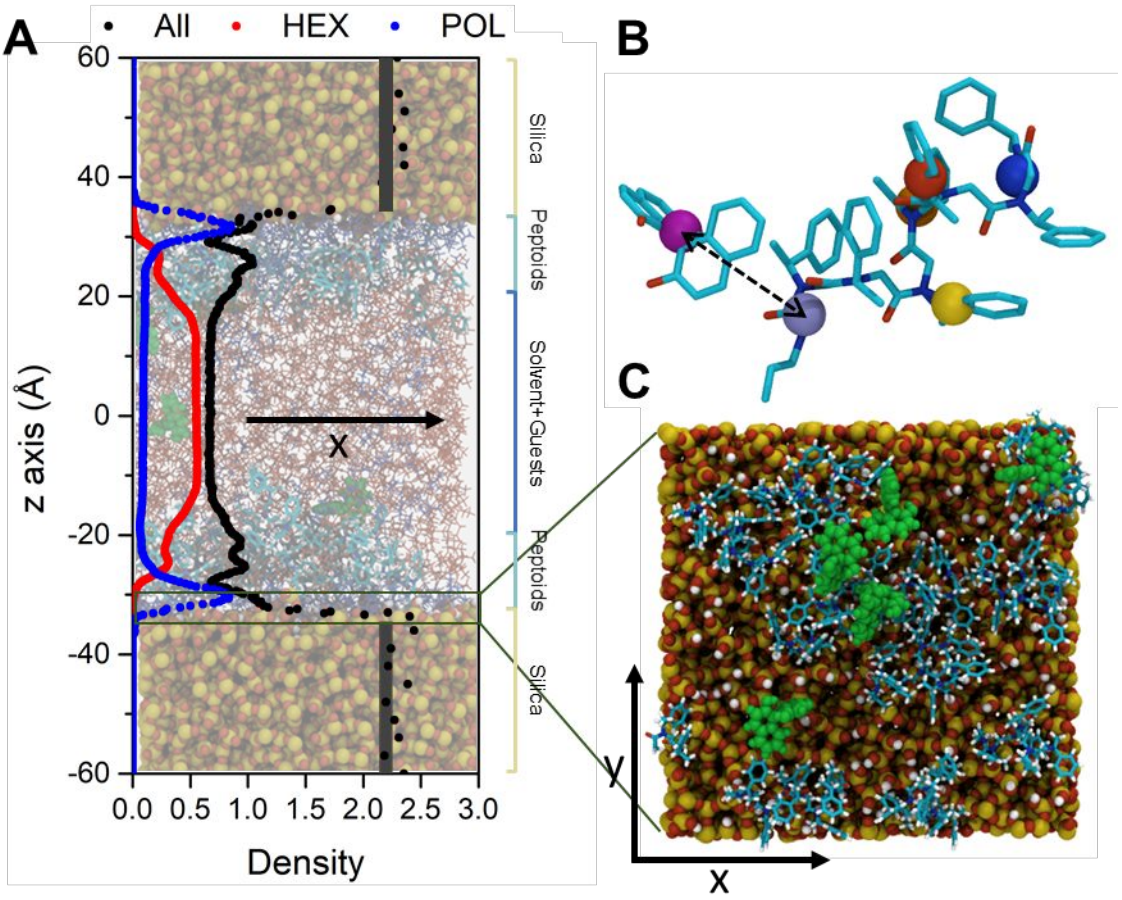

Figure 1. (**A**) Density profile (black dots) along the z axis of the simulation box. The elution occurs along the x axis. The vertical gray bands correspond to the experimental density of amorphous silica. Partial phase segregation of n-hexane (red dots) and 2-propanol (blue dots) is observed on top of the silica surfaces. (**B**) Representation of the distances computed between the center of mass of BINOL and the center of mass of each peptoid residue. (**C**) Top view of the bottom silica surface with grafted peptoids. BINOL molecules are highlighted in green.

The experimental mobile phase is a mixture of n-hexane/2-propanol 70/30 (v/v), which translates in our simulation box into 575 and 425 molecules, respectively, to fill the gap (~ 58 x 58 x 65 Å^3) between the two silica surfaces. Solvent molecules are described here using the CGenFF parameters for the (non-)bonded interactions.[41] Atomic charges were generated using the

ParamChem web server.[42] We chose these parameters because they adequately reproduce the densities of pure solvents as well as the densities of mixtures at different ratios (**see Supporting Information**).

The chiral analytes selected are five (*R*)- and (*S*)-2,2'-bihydroxy-1,1'-binaphthyl (referred to as BINOL in the following). They are also described by the CGenFF parameters, with atomic charges assigned using the ParamChem web server.[42]

MD simulations on the entire system were performed using the NAMD software using 3D periodic boundary conditions, see **Figure 1**.[43] Solvent molecules (n-hexane and 2-propanol), peptoids, guest molecules (BINOL) and the silica atoms closer to the surfaces (within 5 Å) were subjected to thermal motion, while the core of the slab was kept frozen at its equilibrium position to save computational time.[44] No bond constraints were applied on the system. The simulations were systematically carried out on a system containing only a given BINOL enantiomer (*R* or *S*), since a racemic mixture would either reduce the quality of the statistical analysis made on a given enantiomer if keeping the same total number of molecules or increase too much the number of molecules in the box to guarantee that they behave independently. Each simulation was carried out using a timestep of 1 fs. The particle mesh Ewald (PME) method was used to deal with the Coulomb interactions with a real space cutoff of 10 Å and a switching distance of 9.5 Å.[45] The van der Waals interactions are treated by a Lennard-Jones potential (12-6) using a 10 Å cutoff with a switching distance of 9.5 Å, and Lorentz-Berthelot mixing rules. The system was first equilibrated with a Langevin thermostat[46,47] at 300 K and a Langevin barostat[48] set to 1 atm applied only in the z direction (*i.e.*, the length of the box along the x and y axes remain fixed), until reaching the convergence of the density and the energy of the solvent mixture after about 10 ns (**Figure S4, S5**). Then, steered molecular dynamics (SMD)[49] simulations of 650 ns for the *N*spe substrate, and

500 ns for the *N*sar substrate were carried out in the NVT ensemble for samples containing 5 enantiomers (*R* or *S*) using a pulling force of 1.25 kcal.mol^{-1}.Å^{-1} on a single atom (the hydrogen attached to one of the two carbons in α to the hydroxyl moiety) of each guest molecule along the x direction. The pulling force is used to mimic the elution process along the chromatography column. We chose this value because the flow it generates leads a low deviation from the temperature imposed by the thermostat (see **Supporting Information** for details about the evaluation of the effective temperature); moreover, it keeps the elution efficient (*i.e.*, the net flow is not zero) and the computational cost, which is inversely proportional to the pulling force (the lower the force, the longer the time for the analyte to travel a certain distance), reasonable. The convergence of the simulations was monitored ensuring that the moving average of the velocity of each BINOL inside the simulation becomes constant at long enough simulation times.

Conformational Analysis

Since we seek to characterize in a statistical way the conformation of the peptoids involved in the recognition process, we developed a labeling method similar to that proposed by Spencer *et al.*[50] The peptoid backbone is described by 3 dihedral angles per monomer unit (ω, φ and ψ), whose combinations give rise to specific secondary structures. For example, a perfect right-handed helix is characterized by a periodic repetition of the pattern (ω ~ 0°, φ ~ -80°, ψ ~ 180°) (**Figure S7**). The nomenclature is based on the assignment of a given letter to a range of values for each dihedral angle. Spencer *et al.* describe ψ by the capital Greek letter Z, φ by R (right-handed) or S (left-handed) and ω by c (*cis*) or t (*trans*). Accordingly, a helical conformation would be denoted as Z_{Rc}-helix. However, this nomenclature is too restrictive since it is mostly focused on helical geometries. In this work, we extended the nomenclature to include a broader range of possible structures and be able to account for slight structural changes. The complete method is described

in the **Supporting Information**. Briefly, we now associate to each monomer unit a given letter based on the value of the dihedral angles; for example, for values characteristic of a right-handed helix, we simply use the single letter "R". We apply the same method for the different combinations of dihedrals along the peptoid backbone (from N to C terminus) and finally obtain a coded sequence representative of each unit. For sake of illustration, "RRRXX" points to a conformation where the 3 monomer units starting from the N terminus form a right-handed helix, while the last two on the C terminus side, XX, feature any other dihedral combination that is not a right-handed helix. Examples of the most common conformation sequences encountered in the simulations are provided in **Table S4**, while the complete description for each generic name is provided in **Supporting Information** (**Table S3**).

3. Results and discussion

Steered Molecular Dynamics on (S)-BINOL interacting with Nspe

The system under study contains 5 (*S*)-BINOL molecules that were randomly inserted in the solvent layer (**Figure 1A**). A first MD run was conducted using a Langevin piston of 1 atm for 10 ns to equilibrate the system which rapidly reached a density close to the experimental value in the bulk (2.23 versus 2.2 g/cm^3 for silica and 0.67 versus 0.676 g/cm^3 for the solvent),[51] **Figure 1A**). Interestingly, the equilibrated structure displays a certain phase segregation in the density profile between n-hexane and 2-propanol molecules, with the latter forming a layer on top of the silica surface. This is explained by favorable polar interactions between silanol groups and 2-propanol, compared to n-hexane. Such a segregation has also been observed by Monte Carlo simulations performed on alkane-alcohol mixtures, both in the bulk and in confined samples.[29,52,53]

After equilibration of the system, a steered molecular dynamics (NVT, 650 ns, Langevin thermostat, 300 K) was carried out by applying a pulling force of 1.25 kcal.mol^{-1}.Å^{-1} on a single

atom of each of the 5 (*S*)-BINOL molecules along the eluting (x) direction. We checked that this force does not induce a specific orientation of BINOL by measuring the time evolution of the cosine of the angle θ formed between the C-C bond linking the naphthyl moieties, and the cell vectors (**Figures S8 and S9**). The value of cos(θ) in both the y and z directions oscillates between -1 and 1, thus indicating that the BINOL molecules sample all possible orientations. As expected, along the x direction, the value mainly oscillates between 0 and -1 since the pulling force is applied along this direction. We monitored several other parameters along the SMD, such as the x, y, and z coordinates of the center of mass of each (*S*)-BINOL, the conformation of each peptoid chain (20 in total) using the classification described in the section "*Computational Details"*. We also characterized the hydrogen bonds by measuring the distribution $D-H\cdots A$ distances and angles using the HBonds plugin (v1.2) from VMD (starting at 2 up to 4 Å by 0.2 Å steps, and at 20° up to 180° by steps of 20°).[54] For sake of conciseness, we will discuss in detail the time evolution of a single (*S*)-BINOL molecule, while other physical observables are computed as the average over 5 molecules. The analysis of other compounds is reported in the **Supporting Information** (**Figure S10-S15**).

The displacement of the center of mass of each (*S*)-BINOL along the direction x is punctuated by several plateaus ranging from 1 to 10 ns, as shown in the inset of **Figure 2 (see also Supporting Information Figures S10-S15**. These plateaus correspond to periods of time in which BINOL specifically interacts with peptoids near the surface on the two sides of the pore (for |z| > 20 Å), as shown by the correlation between the plateaus along the x-displacement and the position along z, highlighted by the green dashed rectangle in **Figure 2**. To better depict this interaction, we measured the distance between the center of mass of each peptoid and that of the BINOL molecule along the trajectory, as schematized in **Figure 1B**. If this distance is smaller than 7 Å (the value

computed for a van der Waals contact between a BINOL molecule and a peptoid in a right-handed helix conformation), we consider that a contact is established. Note that we also count one single interaction also when several residues of a given peptoid are simultaneously in contact. This analysis indicates that BINOL interacts more often with the C terminus, i.e., the most exposed side, than with the N terminus grafted on silica (**Figure 3A**). The results have been combined into conformational contact maps featuring the time-evolution of the conformation (color coded) of each individual peptoid chain, together with contact events (**Figure 4**). For example, **Figure 4** shows that the plateau along the x and z coordinates at ~ 75 ns, highlighted in **Figure 2**, is linked to the interaction between BINOL and peptoid chains number 13, 16 and 19 adopting a "RRRXX" conformation (partial right-handed helix, with X a wildcard corresponding to any other letter of the code) during this contact event. We next gathered the conformations of each peptoid chain during the contact events along the simulation to compute their relative abundance, see **Table 1**. In doing so, we found that the main conformations involved in contact events are all derived from a perfect right-handed helix (**Figure S16**). The deviation from the perfect right-handed helix mainly arises at the C terminus side (typically the last two residues), where hydrogen bonds can develop between the BINOL molecule and the amide moiety (**Figure 3A**). This is consistent with the hypothesis of Wu *et al.* that one of the ingredient for the enantioselectivity of *N*spe peptoids against BINOL molecules is the formation of hydrogen bonds.[16] To assess this possibility, we computed the distribution of $D-H\cdots A$ distances and angles between donors (D, consisting in BINOL hydroxyl groups and the -NH group at the peptoid C terminus) and acceptors (A, BINOL hydroxyl oxygen and peptoid amide oxygens, **Figure 5**). Clearly, hydrogen bonds can form for all $D-H\cdots A$ pairs, according to standard geometric criteria (distances lower than 3.5 Å, and angle higher than 150°,[55] as highlighted with a white frame in **Figure 5**). The exposure of the amide

hydrogen at the C terminus is then crucial to form hydrogen bonds with (*S*)-BINOL. Moreover, the structural reorganization at the C terminus allows the good positioning of penultimate amide oxygen to form another hydrogen bond with the (*S*)-BINOL, which appears to be the most probable one. As we will see in the next section, the formation of these hydrogen bonds appears to be more frequent for the (*S*)-BINOL than the (*R*)-BINOL.

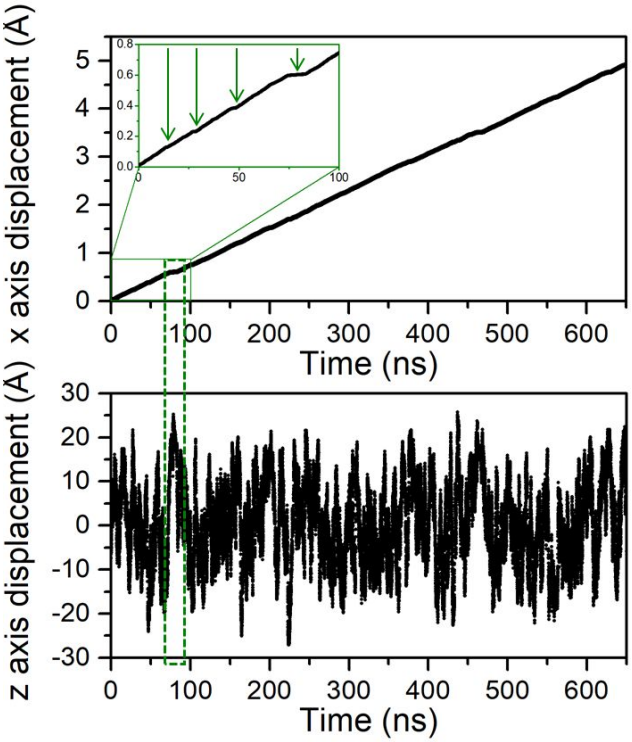

Figure 2. Displacement of a single (*S*)-BINOL molecule along the x (top) and z axis (bottom) over 650 ns. Plateaus are observed along the x displacement as pointed out in the inset by the green arrows, with an associated z displacement towards ± 20-25 Å, *i.e.,* close to the peptoids at the silica surface (highlighted for sake of illustration at ~ 75 ns by a green dashed rectangle).

Table 1. Main conformations adopted by *N*spe and *N*sar peptoids only during contact events with (*R*)- and (*S*)-BINOL molecules. The "X" character is used as wildcard and can be any of the previously defined letter (C, T, M, L), except the one in the current sequence. The complete description of the conformations is available in the **Supporting Information**.

Conformation	(*R*)-BINOL (%)	(*S*)-BINOL (%)
	*N*spe	
RRRRX	29	34
RRRXX	34	25
RRRRr	16	25
Random coil	14	7
	*N*sar	
Random coil	97	97

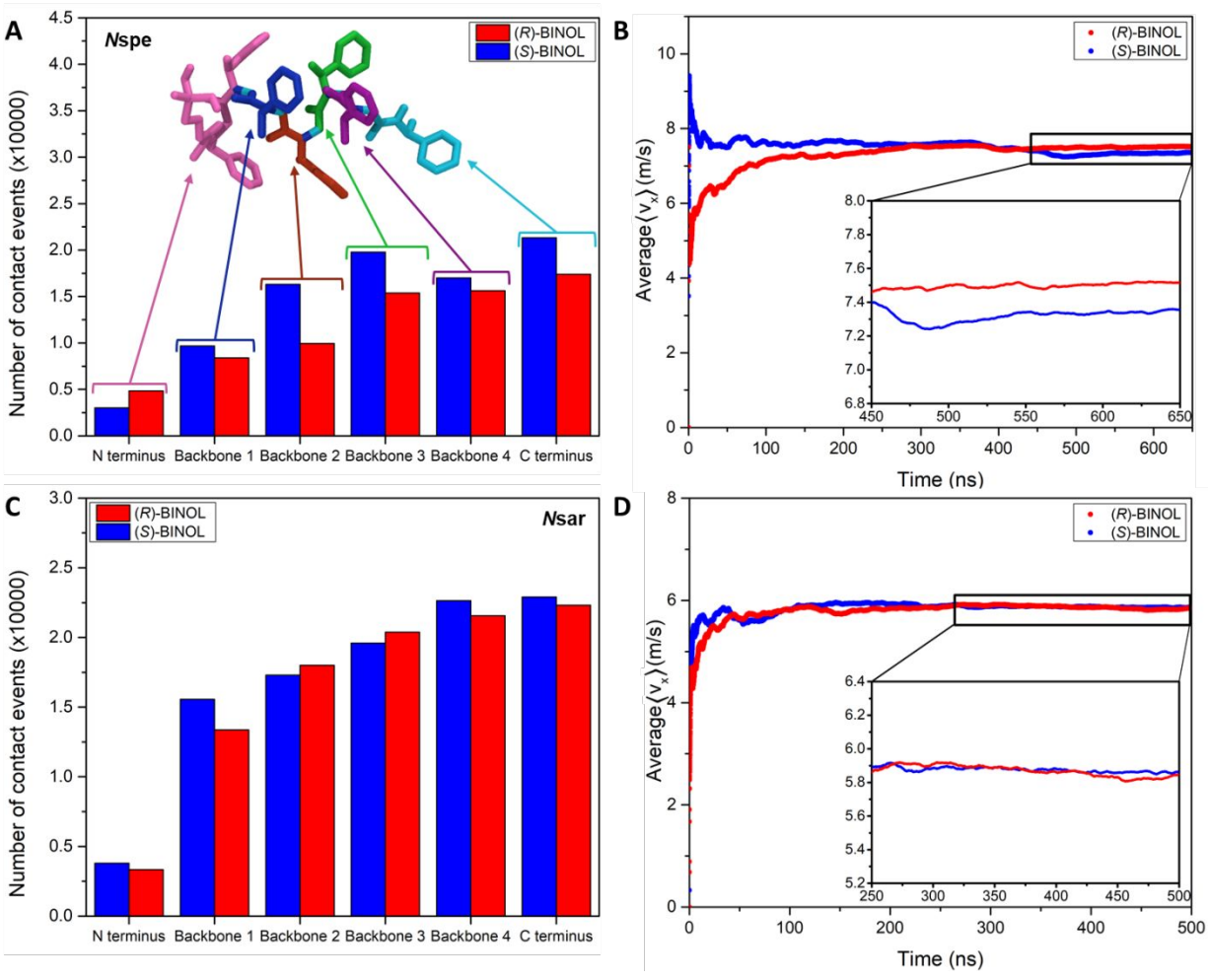

Figure 3. Number of contact events of (*R*)- and (*S*)-BINOL with (**A**) the *Nspe* peptoid residues from the N to C terminus, with most of the interactions occurring on the C terminus side (SMD

run of 650 ns) and (**C**) the *N*sar peptoid residues yielding a more homogeneous distribution (SMD run of 500 ns). (**B**) Evolution of the average velocity of (*R*)- and (*S*)-BINOL interacting with (**B**) the *N*spe peptoids (convergence is reached after 500 ns, as observed in the inset) and (**D**) with the *N*sar peptoids (convergence is reached after 300 ns).

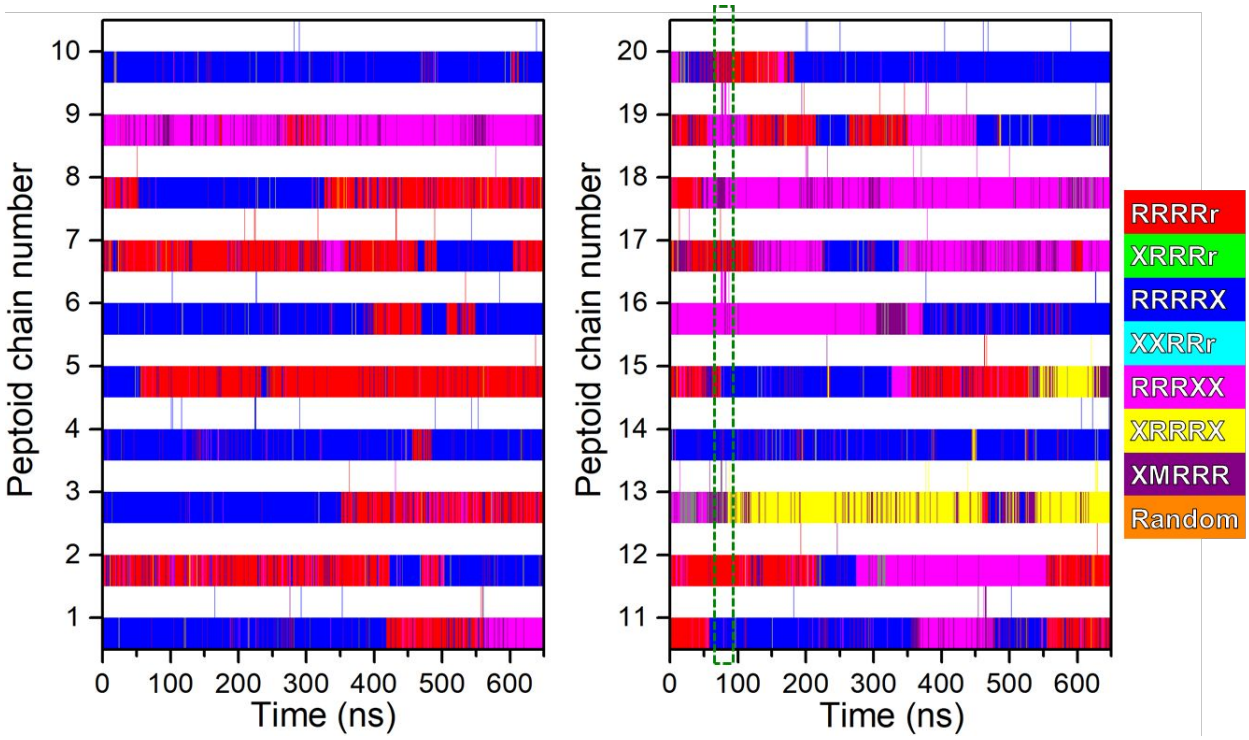

Figure 4. Conformational contact maps of a single (*S*)-BINOL compound with each of the 20 peptoid chains. Each color corresponds to a given peptoid conformation represented by the sequences of letters in the legend, as described in the **Supporting Information**. For every chain number, two colored ribbons are shown, above and below the given number. The lower line depicts the evolution of the conformation along the SMD, while the upper one (mostly white) highlights the conformations occurring when the BINOL molecule is in contact with the peptoid chain.

In order to assess the enantioselectivity, we finally computed the moving average velocity profile for the 5 BINOL molecules, (**Figure 3B)**. For (*S*)-BINOL, the velocity reaches an average value of 7.354 m/s upon convergence (after 500 ns). It is worth stressing that this specific value is

tributary of the chosen pulling force and hence cannot be readily compared to experimental values, just as the experimental elution time depends on instrumental parameters such as the flux of solvent. However, the comparison of the velocity of the two enantiomers in the same theoretical (or experimental) conditions will be meaningful (see below). There are so many interactions occurring in the process of chiral recognition that there is a very slow convergence of the average velocity (calculated from time zero up to a given time t), i.e., the quantity displayed in figure 3. Nevertheless, making our analyses only after 500 ns would make us loose the memory of all interactions that have occurred before and that are instrumental to reach the convergence. For sake of illustration, we report in the Figure S42 and FS43 the time evolution of instantaneous velocities averaged among the (R)- and (S)-binol molecules in presence of Nspe and Nsar peptoids. Doing so, we do not distinguish any convergence or specific trend after 500 ns of the instantaneous velocities since the BINOL molecules are submitted to a Brownian motion and interact sporadically with the peptoid chains. As a result, the instantaneous velocities highly fluctuate and the sole consideration of the results beyond 650 ns cannot make us recover the required convergence due to the poor sampling. Accordingly, this indicates that all dynamical processes before 650 ns are truly part of the chiral selection process and that we need the entire trajectory to ensure convergence, as achieved in Figure 3.

Steered Molecular Dynamics on (R)-BINOL interacting with Nspe

With exactly the same setup used for the *(S)*-BINOL simulation, we next performed a SMD simulation for the pore containing five (*R*)-BINOL molecules, whose trajectories are analyzed in detail in **Figures S18-S23**. In the case of (*R*)-BINOL, we obtained a higher average velocity compared to (*S*)-BINOL (7.515 vs. 7.354 m/s respectively, **Figure 3B**), thus implying that (*S*)-BINOL is characterized by a larger elution time in our virtual chromatographic column. This is fully consistent with the experimental results obtained by Wu *et al.*[16] The difference in the elution times arises from a different occurrence of contact events experienced by the two enantiomers (**Table 1**). since the main peptoid conformations involved during contact events are the same for

both BINOL enantiomers, though their relative abundances are different. (*R*)-BINOL interacts more frequently with helices largely deviating from the ideal right-handed helix (helices of type "RRRRX" and "RRRXX", **Table 1**) as well as with random coil conformations. More importantly, (*R*)-BINOL interacts less frequently with the grafted peptoids than the (*S*)-BINOL (**Figure 3A**). Moreover, we do observe a clear difference when comparing the distribution of $D-H\cdots A$ distances and angles of the same donor-acceptor couples for (*R*)- and (*S*)-BINOL at the C terminus side of the peptoids (**Figure 5**). The probability of forming hydrogen bonds between (*S*)-BINOL and peptoids is much higher (in the range of 2 to 3.5 Å and angles comprised between 150° and 180°) than for (*R*)-BINOL for hydroxyl-amide O2, and N-terminus-hydroxyl oxygen bonds, while it is identical for the hydroxyl-amide O1 interaction.

Besides forming hydrogen bonds, (*S*)-BINOL can interact through π-π interactions inside the cavities formed along the helix backbone, as suggested by Wu *et al.* (**Figure S15A**).[16] In specific helical geometry of type "RRRRX" or 'RRRXX", a pocket is formed at the C terminus side of the peptoid into which the (*S*)-BINOL geometry fits adequately (**Figure S17B**), while such behavior is barely observed along the trajectory for (*R*)-BINOL. By swapping the (*S*)-BINOL in the complex displayed in **Figure S17B** with a (*R*)-BINOL, we observe that (*R*)-BINOL cannot fit equally well inside the cavity (**Figure S17C**).

The consequences of these complex interactions also emerge from the compared analysis of the autocorrelation function of the dihedral angles,[56] $C_\alpha(t) = \langle \cos\alpha(\tau)\cdot\cos\alpha(\tau+t)\rangle + \langle \sin\alpha(\tau)\cdot\sin\alpha(\tau+t)\rangle$, with α corresponding to the main peptoid backbone dihedrals ω, φ and ψ (**Figures S39, S40, Table S2**). Indeed, we observe a major difference in the behavior of the ω dihedral located at the C terminus extremity when comparing (*R*)- and (*S*)-BINOL simulations. In

the former case, ω shows a much shorter correlation time, which we attribute to a re-orientation of the C terminus extremity induced by the formation of hydrogen bonds.

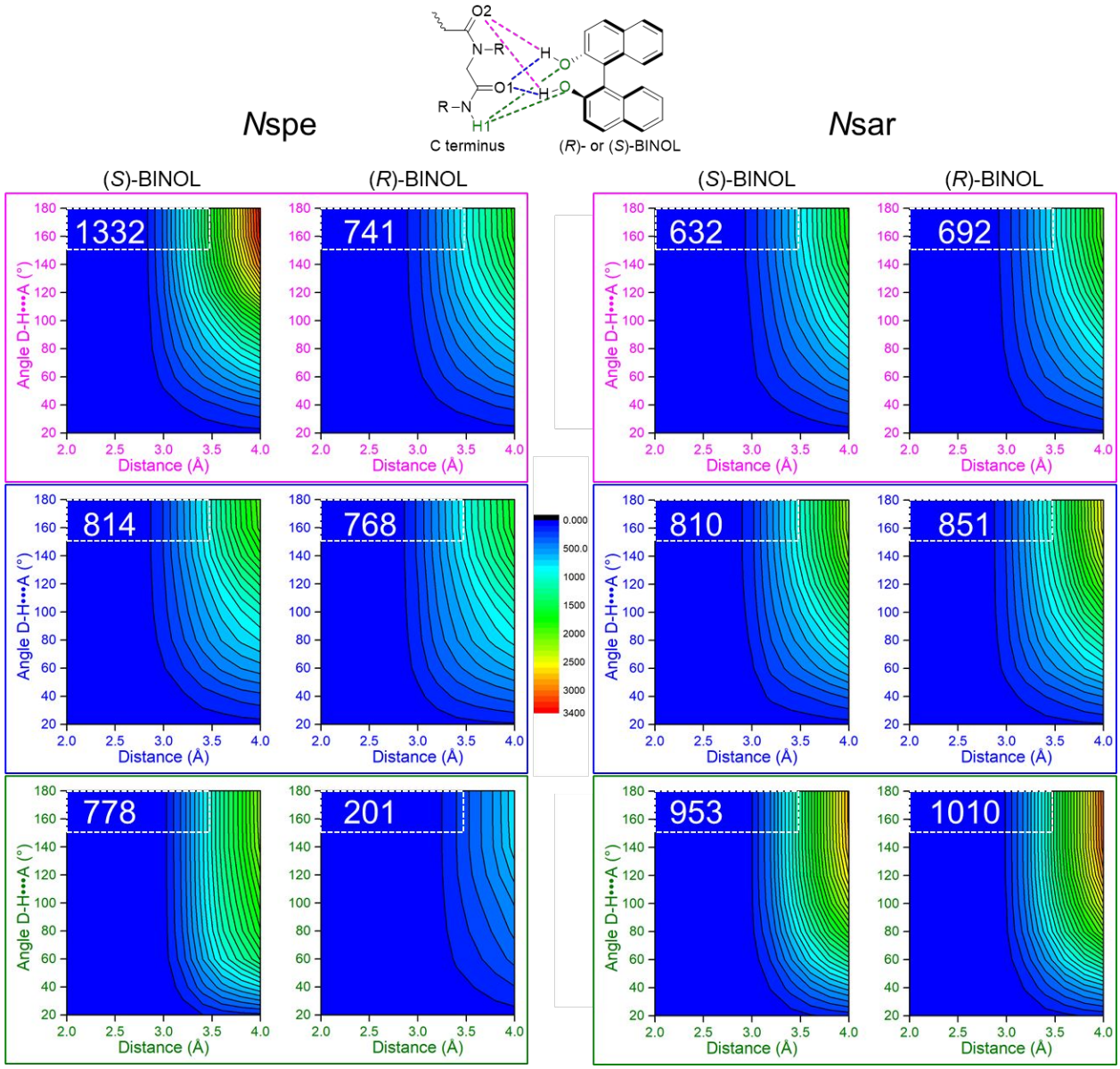

Figure 5. Distributions of angles and distances between donor (D), hydrogen (H) and acceptor (A) of BINOL-peptoid couples. The hydrogen bonds can be formed between the C terminus side (oxygen and hydrogen atoms of amide groups) of peptoids (*N*spe or *N*sar) and (*R*)- or (*S*)-BINOL. Each hydrogen bond couple is represented by colored dashed bonds in the molecular representation

and the corresponding heatmap is identified by its colored frame. The dashed white frame inside the distributions represent the common range used to characterize hydrogen bonds, according to Van Der Spoel *et al*..[55] We also report in this frame the maximum number of hydrogen bonds in this range along the dynamics.

Steered Molecular Dynamics on (S)- or (R)-BINOL: The Nsar case

In order to substantiate the results for the *N*spe peptoids chiral stationary phase discussed above, we performed additional simulations with the same conditions (grafting density, peptoid oligomer length, solvent composition, etc.) on a model system made this time of achiral peptoids, which in principle should not exhibit any enantioselectivity. We chose sarcosine, the simplest possible peptoid unit bearing a methyl side chain, as a building block for an achiral hexamer (*N*sar, **Scheme 1**). Such peptoids are known to behave as flexible polymers and to not adopt any particular conformation in a variety of solvents (polar and apolar); the main conformation type is thus labelled as "random coil".[32,57] The analysis of the displacements of the (*R*)- and (*S*)-BINOL along the x and z axes during the simulations with the *N*sar stationary phase, as well as the conformational contact maps are reported in **Supporting Information** (**Figures S25-S38**). Unlike *N*spe hexamers, BINOL enantiomers interact more homogeneously with the units of the sarcosine chains (except with the hardly accessible N terminus grafted on the silica substrate, **Figure 3C**). This can be rationalized by observing that, as expected, sarcosine oligomers do not assume chiral conformations and are more flexible and less sterically hindered than *N*spe peptoids, which are mainly helical-like. The higher flexibility of *N*sar is reflected both by the larger variations in the average end-to-end distances for sarcosine chains along the dynamics (**Figure S24)** and by the dihedral autocorrelation functions that indicate fast conformational rearrangements (characteristic

timescale of about 10 ns), compared to the *N*spe peptoids that can reach up to 150 ns (**Figure S41, Table S3**).

Although sarcosine oligomers behave as random coils, they can still form hydrogen bonds with BINOL enantiomers. However, compared to the chiral *N*spe peptoids for which the hydrogen bond geometrical parameters are different between the two enantiomers, the probability distributions are very similar for *N*sar with both BINOL enantiomers (**Figure 5**) and do not show any evidence of chiral interaction. As a result, no difference is observed in the average velocities of (*S*)- versus (*R*)-BINOL, owing to the achiral nature of the grafted chains (**Figure 3D**).

4. Conclusions

We put forward a computational methodology, based on steered molecular dynamics simulations, for reproducing a liquid chromatography experiment, and applied it to evaluate the enantioselective properties of chiral *N*spe peptoids against both 2,2'-bihydroxy-1,1'-binaphthyl enantiomers (BINOL).[16] Our results show that, during the elution process, (*S*)-BINOL is retained for a longer time than (*R*)-BINOL in the chromatography column, due to more favorable interactions with *N*spe peptoids in conformations derived from a right-handed helix. The geometric deviation from the perfect right-handed helix that arises on the C terminus side promotes the exposure of the amide hydrogen of *N*spe peptoids and triggers the formation of hydrogen bonds with (*S*)-BINOL. Moreover, the C terminus can form a groove where the (*S*)-BINOL can fit and bind through π-π interactions. We thus conclude that the formation of hydrogen bonds at the C terminus side of the helical peptoids, as suggested by Wu *et al.*[16], plays a pivotal role in the chiral recognition of binaphthyl derivates, although the origin of the chiral selectivity lies in the right-handed conformation of *N*spe peptoids. In a more general perspective, our study delineates how

important is the proper tuning of the chemical structure of the C terminus side, since it could greatly influence the selectivity of peptoids towards a variety of different chiral compounds.

ASSOCIATED CONTENT

Supporting Information.

Additional analyses, figures, tables, computational details and structural description (PDF).

AUTHOR INFORMATION

Corresponding Author

jerome.cornil@umons.ac.be

luca.muccioli@unibo.it

Author Contributions

S. H., O. M. R. and C. T. have performed the computational studies under the supervision of L. M. All authors analyzed the set of data and contributed to the writing of the manuscript. All authors have given approval to the final version of the manuscript.

Funding Sources

Any funds used to support the research of the manuscript should be placed here (per journal style).

Notes

Any additional relevant notes should be placed here.

ACKNOWLEDGMENT

The work in the laboratory for Chemistry of Novel Materials was supported by the European Commission/Région Wallonne (FEDER—BIORGEL project). S.H. and J.C. are, respectively, FRIA and FNRS research fellows. The UMONS MS laboratory acknowledges the Fonds National de la Recherche Scientifique (FRS-FNRS) for continuing support.

ABBREVIATIONS

(*S*)-N-1-phenylethyl, *N*spe ; chiral stationary phase, CSP ; *N*-methyl, *N*sar ; 2,2'-bihydroxy-1,1'-binaphthyl, BINOL ; steered molecular dynamics, SMD ; n-hexane, HEX ; 2-propanol, POL

REFERENCES

(1) Banik, S. D.; Nandi, N. Chirality and Protein Biosynthesis. In *Topics in current chemistry*; 2012; Vol. 333, pp 255–305.

(2) Nguyen, L. A.; He, H.; Pham-Huy, C. Chiral Drugs: An Overview. *Int. J. Biomed. Sci.* **2006**, *2* (2), 85–100.

(3) Shen, Q.; Wang, L.; Zhou, H.; Jiang, H. Di; Yu, L. S.; Zeng, S. Stereoselective Binding of Chiral Drugs to Plasma Proteins. *Acta Pharmacol. Sin.* **2013**, *34* (8), 998–1006.

(4) Kellogg, R. M.; Nieuwenhuijzen, J. W.; Pouwer, K.; Vries, T. R.; Broxterman, Q. B.; Grimbergen, R. F. P.; Kaptein, B.; Crois, R. M.; de Wever, E.; Zwaagstra, K.; van der Laan, A. C. Dutch Resolution: Separationof Enantiomers with Families of Resolving Agents. A Status Report. *Synthesis (Stuttg).* **2003**, No. 10, 1626–1638.

(5) Mohr, J. T.; Krout, M. R.; Stoltz, B. M. Natural Products as Inspiration for the Development of Asymmetric Catalysis. *Nature* **2008**, *455* (7211), 323–332.

(6) Ricci, A. Asymmetric Organocatalysis at the Service of Medicinal Chemistry. *ISRN Org. Chem.* **2014**, *2014*, 1–29.

(7) Gogoi, A.; Mazumder, N.; Konwer, S.; Ranawat, H.; Chen, N. T.; Zhuo, G. Y. Enantiomeric Recognition and Separation by Chiral Nanoparticles. *Molecules* **2019**, *24* (6), 1–31.

(8) Francotte, E. R. Enantioselective Chromatography as a Powerful Alternative for the Preparation of Drug Enantiomers. *J. Chromatogr. A* **2001**, *906* (1–2), 379–397.

(9) Xiao, Y.; Ng, S. C.; Tan, T. T. Y.; Wang, Y. Recent Development of Cyclodextrin Chiral Stationary Phases and Their Applications in Chromatography. *J. Chromatogr. A* **2012**, *1269*, 52–68.

(10) Ikai, T.; Yamamoto, C.; Kamigaito, M.; Okamoto, Y. Immobilized Polysaccharide-Based Chiral Stationary Phases for HPLC. *Polym. J.* **2006**, *38* (2), 91–108.

(11) Haginaka, J. Protein-Based Chiral Stationary Phases for High-Performance Liquid Chromatography Enantioseparations. *J. Chromatogr. A* **2001**, *906* (1–2), 253–273.

(12) Huang, J.; Chen, H.; Li, T. Improvement of Proline Chiral Stationary Phases by Varying Peptide Length and Linker. *J. Chromatogr. A* **2006**, *1113* (1–2), 109–115.

(13) Ohyama, K.; Oyamada, K.; Kishikawa, N.; Arakawa, M.; Ohba, Y.; Kamino, M.; Wada, M.; Nakashima, K.; Kuroda, N. Investigation of Novel Peptide Chiral Selectors Prepared by Solid-Phase Synthesis with a Tert-Butoxycarbonyl Amino Acid. *Chromatographia* **2009**, *70* (9–10), 1501–1504.

(14) Ohyama, K.; Oyamada, K.; Kishikawa, N.; Ohba, Y.; Wada, M.; Maki, T.; Nakashima, K.; Kuroda, N. Preparation and Characterization of Poly(l-Phenylalanine) Chiral Stationary Phases with Varying Peptide Length. *J. Chromatogr. A* **2008**, *1208* (1–2), 242–245.

(15) Ohyama, K.; Oyamada, K.; Kishikawa, N.; Wada, M.; Ohba, Y.; Nakashima, K.; Kuroda, N. Effects of Temperature and Mobile Phase Condition on Chiral Recognition of Poly(l-Phenylalanine) Chiral Stationary Phase. *Chromatographia* **2011**, *74* (5–6), 467–470.

(16) Wu, H.; Liang, T.; Yin, C.; Jin, Y.; Ke, Y.; Liang, X. Enantiorecognition Ability of Peptoids with α-Chiral, Aromatic Side Chains. *Analyst* **2011**, *136* (21), 4409.

(17) Kirshenbaum, K.; Barron, a E.; Goldsmith, R. a; Armand, P.; Bradley, E. K.; Truong, K. T.; Dill, K. a; Cohen, F. E.; Zuckermann, R. N. Sequence-Specific Polypeptoids: A Diverse Family of Heteropolymers with Stable Secondary Structure. *Proc. Natl. Acad. Sci. U. S. A.* **1998**, *95* (8), 4303–4308.

(18) Fowler, S. a; Blackwell, H. E. Structure-Function Relationships in Peptoids: Recent Advances toward Deciphering the Structural Requirements for Biological Function. *Org. Biomol. Chem.* **2009**, *7* (8), 1508–1524.

(19) Sun, J.; Li, Z. Peptoid Applications in Biomedicine and Nanotechnology. In *Peptide Applications in Biomedicine, Biotechnology and Bioengineering*; Elsevier, 2018; pp 183–213.

(20) Statz, A. R.; Meagher, R. J.; Barron, A. E.; Messersmith, P. B. New Peptidomimetic Polymers for Antifouling Surfaces. *J. Am. Chem. Soc.* **2005**, *127* (22), 7972–7973.

(21) Olivier, G. K.; Cho, A.; Sanii, B.; Connolly, M. D.; Tran, H.; Zuckermann, R. N. Antibody-

Mimetic Peptoid Nanosheets for Molecular Recognition. *ACS Nano* **2013**, *7* (10), 9276–9286.

(22) Simon, R. J.; Kania, R. S.; Zuckermann, R. N.; Huebner, V. D.; Jewell, D. a; Banville, S.; Ng, S.; Wang, L.; Rosenberg, S.; Marlowe, C. K. Peptoids: A Modular Approach to Drug Discovery. *Proc. Natl. Acad. Sci. U. S. A.* **1992**, *89* (20), 9367–9371.

(23) Miller, S. M.; Simon, R. J.; Ng, S.; Zuckermann, R. N.; Kerr, J. M.; Moos, W. H. Comparison of the Proteolytic Susceptibilities of Homologous L-Amino Acid, D-Amino Acid, and N-Substituted Glycine Peptide and Peptoid Oligomers. *Drug Dev. Res.* **1995**, *35* (1), 20–32.

(24) Wu, H.; Su, X.; Li, K.; Yu, H.; Ke, Y.; Liang, X. Improvement of Peptoid Chiral Stationary Phases by Modifying the Terminal Group of Selector. *J. Chromatogr. A* **2012**, *1265*, 181–185.

(25) Wu, H.; Li, K.; Yu, H.; Ke, Y.; Liang, X. Investigation of Peptoid Chiral Stationary Phases Varied in Absolute Configuration. *J. Chromatogr. A* **2013**, *1281*, 155–159.

(26) Wu, C. W.; Sanborn, T. J.; Huang, K.; Zuckermann, R. N.; Barron, A. E. Peptoid Oligomers with α-Chiral, Aromatic Side Chains: Sequence Requirements for the Formation of Stable Peptoid Helices. *J. Am. Chem. Soc.* **2001**, *123* (28), 6778–6784.

(27) Zhao, C.; Cann, N. M. The Docking of Chiral Epoxides on the Whelk-O1 Stationary Phase: A Molecular Dynamics Study. *J. Chromatogr. A* **2007**, *1149* (2), 197–218.

(28) Zhao, C. F.; Cann, N. M. Molecular Dynamics Study of Chiral Recognition for the Whelk-O1 Chiral Stationary Phase. *Anal. Chem.* **2008**, *80* (7), 2426–2438.

(29) Ashtari, M.; Cann, N. M. Poly-Proline-Based Chiral Stationary Phases: A Molecular Dynamics Study of Triproline, Tetraproline, Pentaproline and Hexaproline Interfaces. *J. Chromatogr. A* **2012**, *1265*, 70–87.

(30) Peluso, P.; Dessì, A.; Dallocchio, R.; Mamane, V.; Cossu, S. Recent Studies of Docking and Molecular Dynamics Simulation for Liquid-Phase Enantioseparations. *Electrophoresis* **2019**, *40* (15), 1881–1896.

(31) Wang, X.; Jameson, C. J.; Murad, S. Modeling Enantiomeric Separations as an Interfacial Process Using Amylose Tris(3,5-Dimethylphenyl Carbamate) (ADMPC) Polymers Coated on Amorphous Silica. *Langmuir* **2020**, *36* (5), 1113–1124.

(32) Fasman, G. D.; Blout, E. R. Copolymers of L-proline and Sarcosine: Synthesis and Physical-chemical Studies. *Biopolymers* **1963**, *1* (2), 99–109.

(33) Della Valle, R. G.; Andersen, H. C. Molecular Dynamics Simulation of Silica Liquid and Glass. *J. Chem. Phys.* **1992**, *97* (4), 2682–2689.

(34) Roscioni, O. M.; Zannoni, C.; Muccioli, L.; Della Valle, R. G.; Pizzirusso, A.; Ricci, M. Predicting the Anchoring of Liquid Crystals at a Solid Surface: 5-Cyanobiphenyl on Cristobalite and Glassy Silica Surfaces of Increasing Roughness. *Langmuir* **2013**, *29* (28), 8950–8958.

(35) Roscioni, O. M.; Muccioli, L.; Mityashin, A.; Cornil, J.; Zannoni, C. Structural Characterization of Alkylsilane and Fluoroalkylsilane Self-Assembled Monolayers on SiO 2 by Molecular Dynamics Simulations. *J. Phys. Chem. C* **2016**, *120* (27), 14652–14662.

(36) Cygan, R. T.; Liang, J. J.; Kalinichev, A. G. Molecular Models of Hydroxide,

Oxyhydroxide, and Clay Phases and the Development of a General Force Field. *J. Phys. Chem. B* **2004**, *108* (4), 1255–1266.

(37) Hoyas, S.; Lemaur, V.; Duez, Q.; Saintmont, F.; Halin, E.; De Winter, J.; Gerbaux, P.; Cornil, J. PEPDROID: Development of a Generic DREIDING-Based Force Field for the Assessment of Peptoid Secondary Structures. *Adv. Theory Simulations* **2018**, *1* (12), 1800089.

(38) Gasteiger, J.; Marsili, M. A New Model for Calculating Atomic Charges in Molecules. *Tetrahedron Lett.* **1978**, *19* (34), 3181–3184.

(39) Dassault Systèmes BIOVIA, Materials Studio, 18.0, San Diego: Dassault Systèmes, 2018. Dassault Systèmes BIOVIA, Materials Studio, 18.0, San Diego: Dassault Systèmes, 2018.

(40) Armand, P.; Kirshenbaum, K.; Falicov, A.; Dunbrack, R. L.; Dill, K. a; Zuckermann, R. N.; Cohen, F. E. Chiral N-Substituted Glycines Can Form Stable Helical Conformations. *Fold. Des.* **1997**, *2* (6), 369–375.

(41) Vanommeslaeghe, K.; Hatcher, E.; Acharya, C.; Kundu, S.; Zhong, S.; Shim, J.; Darian, E.; Guvench, O.; Lopes, P.; Vorobyov, I.; Mackerell, A. D. CHARMM General Force Field: A Force Field for Drug-like Molecules Compatible with the CHARMM All-Atom Additive Biological Force Fields. *J. Comput. Chem.* **2010**, *31* (4), 671–690.

(42) CGenFF interface at paramchem.org: https://cgenff.umaryland.edu/ (accessed Apr 15, 2019).

(43) Phillips, J. C.; Hardy, D. J.; Maia, J. D. C.; Stone, J. E.; Ribeiro, J. V.; Bernardi, R. C.; Buch, R.; Fiorin, G.; Hénin, J.; Jiang, W.; McGreevy, R.; Melo, M. C. R.; Radak, B. K.;

Skeel, R. D.; Singharoy, A.; Wang, Y.; Roux, B.; Aksimentiev, A.; Luthey-Schulten, Z.; Kalé, L. V.; Schulten, K.; Chipot, C.; Tajkhorshid, E. Scalable Molecular Dynamics on CPU and GPU Architectures with NAMD. *J. Chem. Phys.* **2020**, *153* (4), 044130.

(44) Cruz-Chu, E. R.; Aksimentiev, A.; Schulten, K. Water-Silica Force Field for Simulating Nanodevices. *J. Phys. Chem. B* **2006**, *110* (43), 21497–21508.

(45) Darden, T.; York, D.; Pedersen, L. Particle Mesh Ewald: An N ·log(N) Method for Ewald Sums in Large Systems. *J. Chem. Phys.* **1993**, *98* (12), 10089–10092.

(46) Kubo, R.; Toda, M.; Hashitsume, N. *Statistical Physics II*; Springer Series in Solid-State Sciences; Springer Berlin Heidelberg: Berlin, Heidelberg, 1991; Vol. 31.

(47) Phillips, J. C.; Braun, R.; Wang, W.; Gumbart, J.; Tajkhorshid, E.; Villa, E.; Chipot, C.; Skeel, R. D.; Kalé, L.; Schulten, K. Scalable Molecular Dynamics with NAMD. *J. Comput. Chem.* **2005**, *26* (16), 1781–1802.

(48) Feller, S. E.; Zhang, Y.; Pastor, R. W.; Brooks, B. R. Constant Pressure Molecular Dynamics Simulation: The Langevin Piston Method. *J. Chem. Phys.* **1995**, *103* (11), 4613–4621.

(49) Izrailev, S.; Stepaniants, S.; Balsera, M.; Oono, Y.; Schulten, K. Molecular Dynamics Study of Unbinding of the Avidin-Biotin Complex. *Biophys. J.* **1997**, *72* (4), 1568–1581.

(50) Spencer, R. K.; Butterfoss, G. L.; Edison, J. R.; Eastwood, J. R.; Whitelam, S.; Kirshenbaum, K.; Zuckermann, R. N. Stereochemistry of Polypeptoid Chain Configurations. *Biopolymers* **2019**, *110* (6), 1–6.

(51) Rotter, J. M.; Knickle, H. N. Isobaric Vapor-Liquid Equilibrium Data for the System n-